Applied Physics Letters ARTICLE scitation.org/journal/apl

Semiconductor-to-metal transition in atomic layer deposition (ALD) of VO_2 films using VCl_4 and water

Cite as: Appl. Phys. Lett. **118**, 261902 (2021); doi: 10.1063/5.0053566
Submitted: 8 April 2021 · Accepted: 11 June 2021 ·
Published Online: 29 June 2021

View Online Export Citation CrossMark

Jeya Prakash Ganesan,[1] Durjoy Dev,[2] Adithi Krishnaprasad,[2] Corbin Feit,[1] Daniel Moser,[3] Ravindra K. Kanjolia,[4] Tania Roy,[1,2,5,6] and Parag Banerjee[1,2,7,8,a)]

AFFILIATIONS

[1]Department of Materials Science and Engineering, University of Central Florida, Orlando, Florida 32816, USA
[2]Nanoscience Technology Center (NSTC), University of Central Florida, Orlando, Florida 32816, USA
[3]EMD Electronics, Sheboygan Falls, Wisconsin 53085, USA
[4]EMD Electronics, Haverhill, Massachusetts 01832, USA
[5]Department of Electrical and Computer Engineering, University of Central Florida, Orlando, Florida 32816, USA
[6]Department of Physics, University of Central Florida, Orlando, Florida 32816, USA
[7]Florida Solar Energy Center (FSEC), University of Central Florida, Orlando, Florida 32816, USA
[8]Renewable Energy and Chemical Transformation (REACT), Faculty Cluster Initiative, University of Central Florida, Orlando, Florida 32816, USA

[a)]Author to whom correspondence should be addressed: parag.banerjee@ucf.edu

ABSTRACT

The semiconductor-to-metal transition of vanadium dioxide (VO_2) films is studied using temperature-dependent Raman, optical, and electrical measurements. The VO_2 films are deposited via an atomic layer deposition (ALD) process using alternate pulses of vanadium tetrachloride and H_2O at 350 °C. A growth rate of 0.021 nm/cycle and a thickness of 33 nm of VO_2 are obtained for all films studied. The phase of the film is determined using x-ray diffraction. The as-deposited films are amorphous and are transformed to the monoclinic phase with a post-deposition, forming gas anneal at temperatures $\geq$ 500 °C for 60 min. The purity of the films is determined using x-ray photoelectron spectroscopy and no evidence of residual chlorine is detected. The temperature-dependent Raman A_g mode of the monoclinic VO_2 phase is observed to monotonically decrease from 25 °C to 78 °C; where no evidence of the A_g peak is observed in the film beyond 68 °C. The refractive index and extinction coefficient extracted from temperature-dependent ellipsometry confirm that, beyond 68 °C, free carriers are generated in the film. Electrical measurements performed on a fabricated p++Si/VO_2/Ti/Au device show a semiconductor-to-metal transition behavior with a high resistance of 14701 ± 2284 Ω at 62 °C and a low resistance of 1064.1 ± 143 Ω at 67 °C. This work demonstrates that a halide-based ALD process provides a clean and robust approach to synthesizing high-quality VO_2 films.

Vanadium dioxide (VO_2) undergoes a reversible transition[1] between the semiconducting (monoclinic) and metallic (tetragonal) states at 68 °C. This reversible semiconducting to metallic transition (SMT) can be induced by thermal, electrical, and optical techniques.[2–4] The SMT can be cycled for $\geq 10^6$ times without any degradation to the transition characteristics.[4] Tunability to SMT temperature can be achieved by adding a capping layer such as Al:ZnO.[5] These properties make VO_2 a perfect candidate for electrical/optical switches, thermal sensors, metamaterials, and oscillators.[6–11] VO_2 has been used in smart windows[12] and recently, VO_2 devices have been exploited to emulate neuronal functions in neuromorphic circuits.[13]

The deposition of high quality VO_2 films is a primary requisite for VO_2-based devices. While techniques such as sputtering[14–16] and chemical vapor deposition[17] exist, atomic layer deposition (ALD) produces highly conformal, pinhole free films with atomic scale control over thickness and composition. ALD of VO_2 has been reported with different metalorganic (MO) vanadium precursors. Here, the challenge is to maintain the +4 oxidation state of vanadium in the final film. Precursors such as vanadium tris (N,N′-diisopropylacetamidinate) ($V(amd)_3$): oxidation state of V = +3, tetrakis[ethylmethyamino]vanadium (TEMAV): oxidation state of V = +4, vanadyl oxytriisopropoxide (VTOP): oxidation state of V = +5, and tetrakis[dimethyamino]vanadium (TDMAV): oxidation

state of V = +4 have all been used to deposit VO_2 films.[18–22] An oxidizer molecule (such as H_2O or O_2) is used to eliminate the organic ligands during the ALD half-cycles, while assuring that the vanadium is in its +4 state. Additionally, post-deposition anneals in the temperature range of 400–550 °C convert the as-deposited amorphous film into crystalline VO_2 and eliminate the entrapped carbon impurities (if any) left behind from the MO precursor.[23–25] In cases where the film is partially V_2O_5, annealing in a reducing atmosphere can convert the film fully into VO_2.[18] An outstanding challenge in depositing VO_2 using MO precursors is the associated low vapor pressures of MO precursors, thus making assistive delivery involving precursor heating and inert gas bubbling a necessity.

As an alternative, ALD of VO_2 using halide-based precursors such as vanadium tetrachloride (VCl_4) is highly attractive. Halide-based chemistry has been successful in synthesizing crystalline vanadium oxide films via atmospheric pressure chemical vapor deposition (APCVD),[26–28] and thus, its ALD analog may provide advantages over the MO precursor approach. First, the oxidation state of vanadium in the precursor is fixed at +4. An oxidizer such as H_2O can break a thermally activated V–Cl bond. Second, the film by-product (i.e., HCl) is gaseous and can be removed during purge steps, i.e., stoichiometrically pure films can be obtained. Third, halide precursors have a significantly high vapor pressure (e.g., VCl_4 vapor pressure at room temperature = 7.63 Torr)[29] and this relaxes vapor delivery requirements. Taken together, the advantages presented by halide precursors for the ALD of VO_2 are attractive enough to warrant an investigation of the process and the deposited film.

Therefore, in this work, we focus on the structure and properties of ALD VO_2 film deposited using VCl_4 and H_2O chemistry, deposited at a temperature of 350 °C. We note that there has been one report till date on halide-based ALD VO_2, where surprisingly, the authors reported obtaining as-deposited, crystalline VO_2 films.[30] However, in our case, and following a similar protocol, the as-deposited films were found to be amorphous and require an annealing step (≥500 °C for 60 min using forming gas (90% N_2/10% H_2)) to convert to a monoclinic VO_2 film. The monoclinic VO_2 films were characterized through temperature-dependent Raman spectroscopy, x-ray photoelectron spectroscopy (XPS), temperature-dependent spectroscopic ellipsometry (SE), and temperature-dependent electrical resistivity measurements. The results presented in this paper confirm the successful halide-based ALD of stoichiometric VO_2, which in its annealed monoclinic VO_2 state has a SMT at 68 °C.

A Fiji Gen2 plasma-enhanced ALD (PEALD) system from Veeco® was used to deposit VO_2 films on Si p++ wafer. The base pressure on this system (using a turbo-mechanical backing pump) is 5×10^{-7} Torr, and thus, the chamber can achieve a very low partial pressure of O_2 in its idle state. The wafers were ultrasonically cleaned using isopropyl alcohol (IPA) and water followed by 5 min of UV-O_3 cleaning (Ossila®). While the details of the ALD process will be described elsewhere, here the basic recipe for the process is presented. The ALD recipe consisted of alternate supply of VCl_4 (99.99 % from EMD Electronics) and de-ionized (DI) H_2O as precursors. Both the precursors were maintained at room temperature and did *not* require assistive delivery. The dosing rates of VCl_4 and H_2O were 0.06 s with an argon purge of 8 s separating the pulses. It was verified that pulsing for higher times resulted in a saturated growth rate. The deposition temperature was maintained at 350 °C and a base pressure of ∼75 mTorr was maintained during the entire process. The deposition temperature was determined from a previous publication.[30] A VCl_4 pulse provided a spike in pressure to 83 mTorr, whereas the H_2O pulse produced a spike to 135 mTorr. A linear growth rate of 0.021 nm/cycle was recorded using thickness measured via spectroscopic ellipsometry (SE), which is slightly lower than the previously reported value (0.03 nm/cycle).[30] The final thickness of all films evaluated in this work was 33 nm. A Horiba® LabRam Evolution system was used to perform atomic force microscopy to verify the film thickness using scratch and scan method. This is given in supplementary material Fig. S1.

A SE from J. A. Woollam®-M-2000, with a wavelength range from 190 to 1690 nm, was used to optically characterize the film. The optical models for thin film analysis were built in the Complete Ease® software and consisted of a Tauc-Lorentz oscillator and five Lorentz oscillators.[31] *Ex situ* ellipsometric spectra of the VO_2 film were measured at room temperature to obtain growth rate of the films during the ALD process. Additionally, temperature-dependent SE measurements were made from 24 °C to 80 °C to optically study the SMT behavior in crystallized VO_2 films and obtain the real (i.e., "n") and imaginary parts (i.e., extinction coefficient, "k") of the refractive index. Raman spectroscopy was performed on a WITec® 300RA confocal Raman system with excitation laser at 532 nm, 20× objective, and a laser power of 3.2 MW/cm^2. All spectra were recorded with 1800 grating. Temperature-dependent Raman measurements were performed using a homebuilt, custom hot stage, capable of performing measurements from room temperature to 200 °C. A Panalytical® Empyrean system with a Cu Kα excitation (Omega = 5° incidence angle) was used to determine the crystallinity of the ALD film via grazing incidence XRD (GIXRD). X-ray photoelectron spectroscopy (XPS) was conducted on as-deposited and annealed samples using a Physical Electronics® 5400 ESCA. The detection limit on this instrument is 0.1 at. %. The beam used was a monochromated Al K_α beam (1486.6 eV). The analysis beam spot size was 200 μm. Samples were argon-ion beam etched to clean the surface of adventitious contaminants and remove surface oxidation effects.

Patterned Ti/Au (5/100 nm) contact pads were deposited on top of the VO_2 film using an e-beam evaporator. The area of the individual electrode was 200×200 μm^2. For electrical measurements, the current–voltage (IV) characterization was performed using a Keysight B1500A semiconductor device parameter analyzer attached to a Janis® cryogenic probe station. The measurement was carried out in vacuum (0.075 mTorr) and a Lakeshore temperature controller (Model 336) was used to perform the temperature-dependent study.

Figure 1(a) shows the Raman spectra of as-deposited and annealed (500 °C and 550 °C) VO_2 samples. The Raman peak at 520.5 cm^{-1}, which corresponds to the Si substrate, is eliminated for clarity. The as-deposited film shows no Raman peaks indicating amorphous VO_2 phase. This was also confirmed by grazing incidence x-ray diffraction, to be shown later. ALD deposited VO_2 films require a post-deposition annealing process to convert the film into crystalline VO_2.[32–36] Therefore, amorphous VO_2 was annealed at 500 °C and 550 °C for 60 min using forming gas. Both annealing temperatures yielded crystalline monoclinic VO_2 film. Raman spectrum with bands at 192, 224, 259, 306, 336, 385, 440, and 616 cm^{-1} are assigned to the monoclinic VO_2 phase.[37] While both annealed samples show the presence of the monoclinic phase, the Raman data clearly show that the

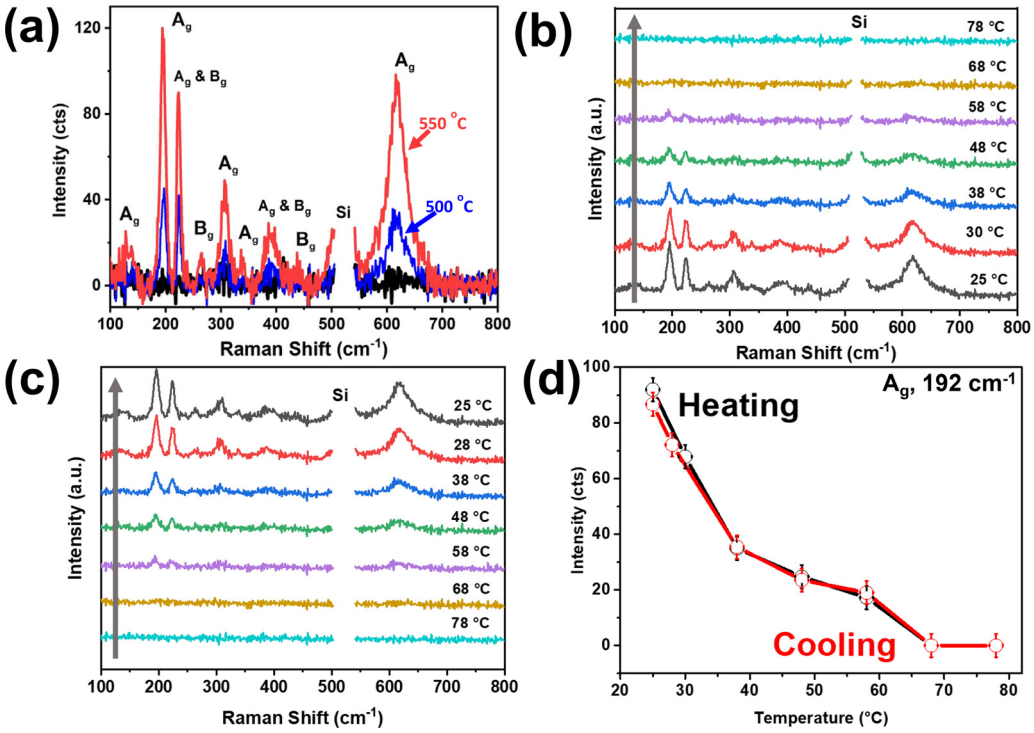

FIG. 1. (a) Raman spectra of the as-deposited sample (black) with no peaks indicating amorphous VO_2 phase, annealed samples: 500 °C (blue) and 550 °C (red) with crystalline Raman peaks indicating VO_2 monoclinic phase. (b) Temperature-dependent Raman spectra during heating cycle. (c) Temperature-dependent Raman spectra during cooling cycle. (d) Temperature-dependent intensity variation of Raman A_g mode at 192 cm^{-1}.

crystallization is pronounced in the film annealed at 550 °C, as compared to the 500 °C sample.

Figure 1(b) shows the temperature-dependent Raman measurement of the 550 °C annealed VO_2 sample during heating, recorded from 25 °C to 78 °C. As the temperature increases, the intensity of Raman bands at 192, 224, and 616 cm^{-1} decrease. At 68 °C, the Raman peaks cannot be observed over the background, indicating that the phase transition of VO_2 from monoclinic to tetragonal is complete.[38] Figure 1(c) shows the temperature-dependent measurement of the 550 °C annealed VO_2 film for the cooling cycle from 78 °C to 25 °C. The emergence of the monoclinic phase can be seen at 58 °C and lower, demonstrating that the SMT transition is reversible. The combined effect of heating and cooling cycles is shown in Fig. 1(d) where the peak intensity of the A_g phonon mode of the monoclinic phase (i.e., at 192 cm^{-1}) is shown. The peak intensities overlap during the heating and cooling cycles. Additionally, it can be seen that past 68 °C the intensity associated with the monoclinic phase is ~0.

Figure 2(a) shows the grazing incidence GIXRD spectrum of as-deposited and annealed VO_2 films. The as-deposited ALD film shows no peaks related to crystalline VO_2, indicating that the film is amorphous in nature. After annealing at ≥ 500 °C for 60 min (500 °C and 550 °C in Fig. 2(a)] using forming gas, a sharp peak is observed at $2\theta = 27.9°$ indicating crystalline VO_2 films.[31] The peak at 27.9° is a result of (011) reflection of VO_2 monoclinic phase.[18] XPS survey spectra (not shown) analysis was done on the Thermo Scientific Avantage® software and the elemental analysis shows an atomic % of V = 30.13% and O = 64.27%, indicating that the annealed film is near stoichiometric at $VO_{2.13}$. Chlorine signal was below the detection limit (≤0.1 at. %) indicating a very clean ALD process with no residual Cl in the film. The XPS survey spectra as well as the chlorine fine spectra of the as-deposited sample are

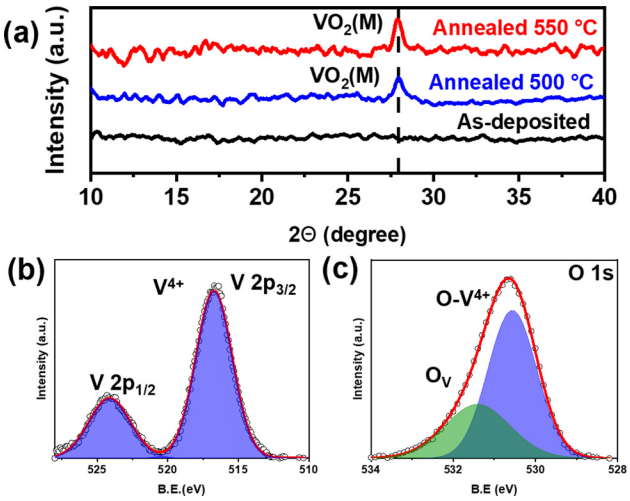

FIG. 2. (a) GIXRD of as-deposited and annealed (500 and 550 °C) VO_2 films. (b) XPS fine spectra of the annealed (550 °C) VO_2 film after sputtering with V 2p showing V^{4+} state. (c) XPS fine spectra of the annealed (550 °C) VO_2 film after sputtering with deconvolution of O 1s peak into O-V^{4+} and O_V.

given in supplementary material Fig. S2. Representative XPS fine spectra of V and O of the 550 °C annealed film (sputtered to remove ambient/surface effects) are shown in Figs. 2(b) and 2(c), respectively. Two peaks at 516.7 and 524.1 eV correspond to $V2p_{3/2}$ and $V2p_{1/2}$ and show only the V^{4+} oxidation state[37] with a spin–orbit splitting (SOS) of 7.4 eV. In Fig. 2(c), the O 1s spectrum is deconvoluted into two peaks. The binding energy at 530.5 corresponds to O^{2-} species bound to V^{4+} and the secondary peak at 531.4 eV is associated with oxygen vacancies (O_V) that may have formed during the forming gas annealing process.[37,39,40]

Having established the structure, phase and stoichiometry of the annealed VO_2 films, temperature-dependent optical and electrical measurements were performed to ascertain the SMT behavior. Here, we focus on the SMT behavior of the 550 °C sample. The temperature-dependent SE was used to extract the *n* and *k* and is presented as contour plots in Figs. 3(a) and 3(b), respectively, as a function of wavelength (*x*-axis) and temperature (*y*-axis). The *n* and *k* are extracted from the CompleteEase® software based off the optical model for VO_2. We report the value of *n* at 633 nm varying from 2.65 to 2.16 for temperatures 25 °C to 80 °C, respectively similar to those reported in literature.[41] At 68 °C, the *n* at 633 nm abruptly decreases from 2.62 to 2.55. The decrease in *n* is even more pronounced in the near IR (NIR) regime, indicating the impact of SMT on the optical properties. In Fig. 3(b), *k* shows a similar effect with temperature, where an abrupt increase is observed at 68 °C across the spectral range, 853–1693 nm. The *k* at 1100 nm is 0.55 at 25 °C but 1.46 at 80 °C, respectively. The extinction coefficient increases significantly in the NIR due to the presence of free electrons.[42] The contour plots of temperature-dependent SE provide the clearest and most sensitive demarcation of the SMT temperature.

To study the impact of SMT on the electrical properties, temperature-dependent IV characteristics are shown on a semi-log plot in Fig. 3(c) for a p++Si/VO_2/Ti/Au Si device. For this example, the 550 °C—60 min annealed VO_2 film was used as the active layer. The temperature was varied from 27 °C to 127 °C. The low temperature (27 °C–62 °C) IV characteristics are closely spaced together, where the current density at 3 V was recorded to be 0.219 ± 0.07 A/cm^2. From 67 °C to 127 °C, the current shows an abrupt rise and the current density at 3 V is 21.22 ± 8.41 A/cm^2. To highlight this effect even further, the temperature dependent resistance is shown in Fig. 3(d). The resistance decreases as temperature is increased and the drop at ∼67 °C (from 14 701 ± 2284 Ω at 62 °C to 1064.1 ± 143 Ω at 67 °C) indicates the phase transition of VO_2 from monoclinic to tetragonal. On cooling, the opposite trend is observed. A slight hysteresis is observed between the heating and cooling curves. It has been suggested that the width of the hysteresis is related to the quality of the VO_2 film.[43,44] This result is in line with the Raman and SE data, indicating that the well-developed

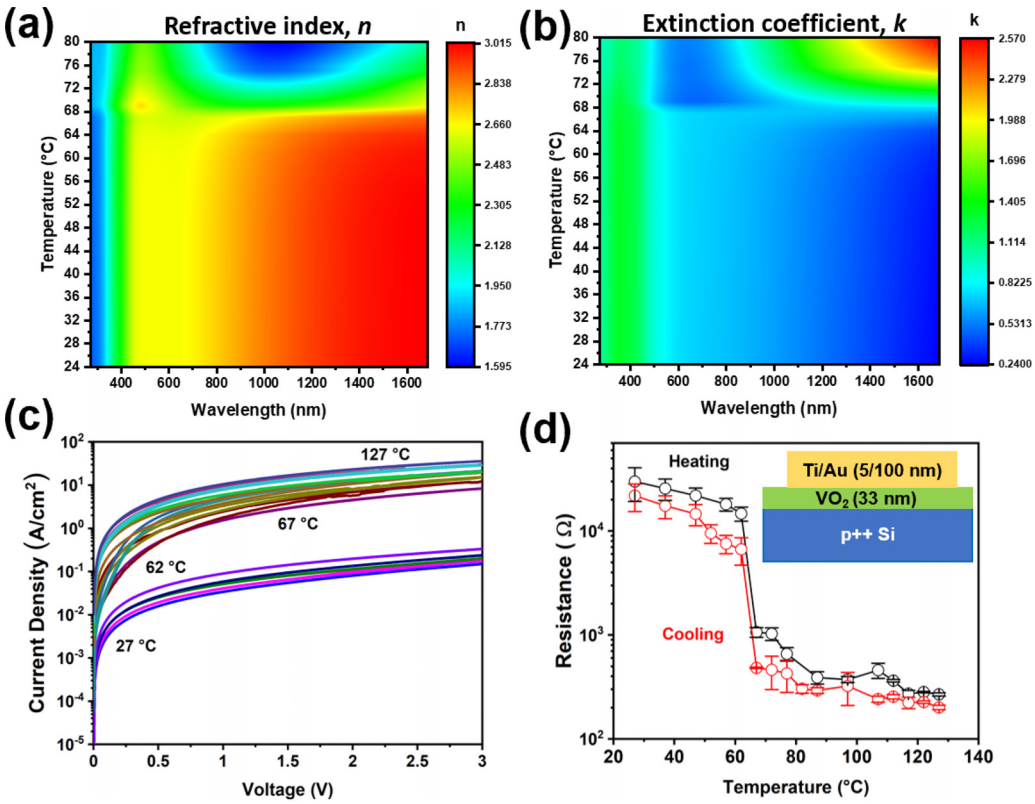

FIG. 3. (a) Temperature-dependent refractive index (n) of the annealed 550 °C sample. (b) Temperature-dependent extinction coefficient (k) of the annealed 550 °C sample. (c) Temperature-dependent IV characteristics (current density vs voltage). (d) Temperature-dependent resistance of the device fabricated with the 550 °C annealed film. The inset shows the schematic of the fabricated device.

monoclinic phase is formed using the $VCl_4 + H_2O$ ALD chemistry followed by forming gas annealing.

Here, we note that our results are in contrast with a recent report from Lee and Chang,[30] where it is shown that a $VCl_4 + H_2O$ ALD process at 350 °C produces a well-developed monoclinic phase without the need for a post-deposition anneal. Our experimental results show, however, that the as-deposited films are amorphous and do require a post-deposition anneal, in line with other reported ALD precursor chemistries for VO_2.

In conclusion, we have demonstrated a halide-based chemistry to deposit amorphous ALD VO_2 films at 350 °C. While details of the ALD process will be discussed in a subsequent publication, here we show that high-quality stoichiometric and crystalline VO_2 films are produced that are free of contaminants, such as chlorine or carbon. The deposition rate is 0.021 nm/cycle. A post-deposition anneal of *at least* 500 °C for 60 min in forming gas crystallizes the VO_2 to its monoclinic phase. The SMT behavior is monitored using Raman, SE, and electrical measurements and the films show a SMT temperature of 68 °C. Availability of a halide-based ALD process provides a broader and simpler choice of chemistry to synthesize high-quality VO_2 films for its ever-growing myriad applications.

See the supplementary material for the verification of VO_2 film thickness via atomic force microscope (AFM) scratch and scan method. The XPS survey spectra and the chlorine 2p fine spectra of the as-deposited film are provided.

J.P.G. was supported by National Science Foundation (NSF) Award No. 1922984. C.F. was supported by NSF Award No. 1908167. The work was partially supported by NSF CAREER Award No. 1845331. The NSF Major Research Instrumentation (MRI) Award No. 1726636 for measuring XPS spectra and NSF MRI Award No. 1920050 for the use of Horiba® LabRam Evolution are acknowledged. The authors wish to thank Professor Laurene Tetard for the use of the Raman system. The use of Advanced Materials Processing and Characterization (AMPAC) facilities and Mr. Kirk Scammon's help at the University of Central Florida is acknowledged.

DATA AVAILABILITY

The data that support the findings of this study are available from the corresponding author upon reasonable request.

REFERENCES

[1] K. Liu, S. Lee, S. Yang, O. Delaire, and J. Wu, Mater. Today **21**(8), 875 (2018).
[2] Z. Yang, C. Ko, and S. Ramanathan, Annu. Rev. Mater. Res. **41**(1), 337 (2011).
[3] A. Pergament, A. Crunteanu, A. Beaumont, G. Stefanovich, and A. Velichko, in EMN Meeting on Computation and Theory (2016).
[4] A. Crunteanu, J. Givernaud, J. Leroy, D. Mardivirin, C. Champeaux, J. C. Orlianges, A. Catherinot, and P. Blondy, Sci. Technol. Adv. Mater. **11**(6), 065002 (2010).
[5] J. R. Skuza, D. W. Scott, R. M. Mundle, and A. K. Pradhan, Sci. Rep. **6**, 21040 (2016).
[6] M. Brahlek, L. Zhang, J. Lapano, H. Zhang, R. Engel-Herbert, N. Shukla, S. Datta, H. Paik, and D. G. Schlom, MRS Commun. **7**(1), 27 (2017).
[7] N. Shukla, A. V. Thathachary, A. Agrawal, H. Paik, A. Aziz, D. G. Schlom, S. K. Gupta, R. Engel-Herbert, and S. Datta, Nat. Commun. **6**(1), 7812 (2015).
[8] N. Shukla, A. Parihar, M. Cotter, M. Barth, X. Li, N. Chandramoorthy, H. Paik, D. G. Schlom, V. Narayanan, A. Raychowdhury, and S. Datta, in *Presented at the 2014 IEEE International Electron Devices Meeting* (unpublished) (2014).
[9] Q. Gu, A. Falk, J. Wu, L. Ouyang, and H. Park, Nano Lett. **7**(2), 363 (2007).
[10] Z. Yang, C. Ko, V. Balakrishnan, G. Gopalakrishnan, and S. Ramanathan, Phys. Rev. B **82**(20), 205101 (2010).
[11] M. Seo, J. Kyoung, H. Park, S. Koo, H. Kim, H. Bernien, B. J. Kim, J. H. Choe, Y. H. Ahn, H. Kim, N. Park, Q. H. Park, K. Ahn, and D. Kim, Nano Lett. **10**(6), 2064 (2010).
[12] Y. Cui, Y. Ke, C. Liu, Z. Chen, N. Wang, L. Zhang, Y. Zhou, S. Wang, Y. Gao, and Y. Long, Joule **2**(9), 1707 (2018).
[13] J. Lin, S. Guha, and S. Ramanathan, Front. Neurosci. **12**, 856 (2018).
[14] C. H. Griffiths and H. K. Eastwood, J. Appl. Phys. **45**(5), 2201 (1974).
[15] K. Okimura, J. Sakai, and S. Ramanathan, J. Appl. Phys. **107**(6), 063503 (2010).
[16] M. Kumar, J. P. Singh, K. H. Chae, J. Park, and H. H. Lee, Superlattices Microstruct. **137**, 106335 (2020).
[17] M. Ibisate, D. Golmayo, and C. López, J. Opt. A **10**(12), 125202 (2008).
[18] P. A. Premkumar, M. Toeller, I. P. Radu, C. Adelmann, M. Schaekers, J. Meersschaut, T. Conard, and S. V. Elshocht, ECS J. Solid State Sci. Technol. **1**(4), P169 (2012).
[19] M. S. Weimer, I. S. Kim, P. Guo, R. D. Schaller, A. B. F. Martinson, and A. S. Hock, Chem. Mater. **29**(15), 6238 (2017).
[20] G. Rampelberg, M. Schaekers, K. Martens, Q. Xie, D. Deduytsche, B. D. Schutter, N. Blasco, J. Kittl, and C. Detavernier, Appl. Phys. Lett. **98**(16), 162902 (2011).
[21] X. Lv, Y. Cao, L. Yan, Y. Li, and L. Song, Appl. Surf. Sci. **396**, 214 (2017).
[22] X. Wang, Z. Guo, Y. Gao, and J. Wang, J. Mater. Res. **32**(1), 37 (2017).
[23] P. Dagur, A. U. Mane, and S. A. Shivashankar, J. Cryst. Growth **275**(1), e1223 (2005).
[24] I. M. Povey, M. Bardosova, F. Chalvet, M. E. Pemble, and H. M. Yates, Surf. Coat. Technol. **201**(22), 9345 (2007).
[25] V. P. Prasadam, B. Dey, S. Bulou, T. Schenk, and N. Bahlawane, Mater. Today Chem. **12**, 332 (2019).
[26] M. N. Field and I. P. Parkin, J. Mater. Chem. **10**(8), 1863 (2000).
[27] D. Vernardou, M. E. Pemble, and D. W. Sheel, Chem. Vapor Depos. **12**(5), 263 (2006).
[28] D. Vernardou, M. E. Pemble, and D. W. Sheel, Thin Solid Films **515**(24), 8768 (2007).
[29] T. E. Daubert and R. P. Danner (1992). "Physical and thermodynamic properties of pure chemicals: Data compilation," American Institute of Chemical Engineers.
[30] W. Lee and Y. Chang, Coat. **8**(12), 431 (2018).
[31] Y. Huang, D. Zhang, Y. Liu, J. Jin, Y. Yang, T. Chen, H. Guan, P. Fan, and W. Lv, Appl. Surf. Sci. **456**, 545 (2018).
[32] C. Kim, S. H. Kim, S. J. Kim, and K. An, Appl. Surf. Sci. **313**, 368 (2014).
[33] M. N. Colpaert, P. Clauws, L. Fiermans, and J. Vennik, Surf. Sci. **36**(2), 513 (1973).
[34] S. Guimond, J. M. Sturm, D. Göbke, Y. Romanyshyn, M. Naschitzki, H. Kuhlenbeck, and H. Freund, J. Phys. Chem. C **112**(31), 11835 (2008).
[35] D. S. Su and R. Schlögl, Catal. Lett. **83**(3), 115 (2002).
[36] D. Q. Liu, W. W. Zheng, H. F. Cheng, and H. T. Liu, Adv. Mater. Res. **79–82**, 747 (2009).
[37] F. Ureña-Begara, A. Crunteanu, and J. Raskin, Appl. Surf. Sci. **403**, 717 (2017).
[38] R. Srivastava and L. L. Chase, Phys. Rev. Lett. **27**(11), 727 (1971).
[39] J. Mendialdua, R. Casanova, and Y. Barbaux, J. Electron. Spectrosc. Relat. Phenom. **71**(3), 249 (1995).
[40] X. Zhang, J. Qin, Y. Xue, P. Yu, B. Zhang, L. Wang, and R. Liu, Sci. Rep. **4**(1), 4596 (2015).
[41] R. T. Kivaisi and M. Samiji, Sol. Energy Mater. Sol. Cells **57**(2), 141 (1999).
[42] T. V. Son, V. V. Truong, P. A. Do, and A. Haché, AIP Adv. **6**(8), 085102 (2016).
[43] X. Xu, X. He, H. Wang, Q. Gu, S. Shi, H. Xing, C. Wang, J. Zhang, X. Chen, and J. Chu, Appl. Surf. Sci. **261**, 83 (2012).
[44] M. M. Qazilbash, M. Brehm, B. G. Chae, P. C. Ho, G. O. Andreev, B. J. Kim, S. J. Yun, A. V. Balatsky, M. B. Maple, F. Keilmann, H. T. Kim, and D. N. Basov, Science **318**(5857), 1750 (2007).